AD-A153 150

DTIC ACCESSION NUMBER

PHOTOGRAPH THIS SHEET

III

LEVEL

1

INVENTORY

DNA-TR-83-43

DOCUMENT IDENTIFICATION

1 Nov 1983

DISTRIBUTION STATEMENT A
Approved for public release;
Distribution Unlimited

DISTRIBUTION STATEMENT

ACCESSION FOR	
NTIS GRA&I	☒
DTIC TAB	☐
UNANNOUNCED	☐
JUSTIFICATION	
BY	
DISTRIBUTION /	
AVAILABILITY CODES	
DIST	AVAIL AND/OR SPECIAL
A-1	

DISTRIBUTION STAMP

DATE ACCESSIONED

DATE RETURNED

85 05 01 37

DATE RECEIVED IN DTIC

REGISTERED OR CERTIFIED NO.

20000807104

PHOTOGRAPH THIS SHEET AND RETURN TO DTIC-DDAC

DTIC FORM 70A

DOCUMENT PROCESSING SHEET

PREVIOUS EDITION MAY BE USED UNTIL STOCK IS EXHAUSTED

DNA-TR-83-43

THE IMPACT OF STRONG SCINTILLATION ON SPACE BASED RADAR DESIGN-NONCOHERENT DETECTION

Dennis L. Knepp
Roger A. Dana
Mission Research Corporation
P.O. Drawer 719
Santa Barbara, California 93102

1 November 1983

Technical Report

CONTRACT No. DNA 001-83-C-0021

THIS WORK WAS SPONSORED BY THE DEFENSE NUCLEAR AGENCY
UNDER RDT&E RMSS CODE B322033466 S99QMXBA00001 H2590D.

Prepared for
Director
DEFENSE NUCLEAR AGENCY
Washington, DC 20305

Destroy this report when it is no longer needed. Do not return to sender.

PLEASE NOTIFY THE DEFENSE NUCLEAR AGENCY, ATTN: STTI, WASHINGTON, D.C. 20305, IF YOUR ADDRESS IS INCORRECT, IF YOU WISH TO BE DELETED FROM THE DISTRIBUTION LIST, OR IF THE ADDRESSEE IS NO LONGER EMPLOYED BY YOUR ORGANIZATION.

UNCLASSIFIED

SECURITY CLASSIFICATION OF THIS PAGE (When Data Entered)

REPORT DOCUMENTATION PAGE	READ INSTRUCTIONS BEFORE COMPLETING FORM
1. REPORT NUMBER: DNA-TR-83-43	2. GOVT ACCESSION NO. / 3. RECIPIENT'S CATALOG NUMBER
4. TITLE (and Subtitle): THE IMPACT OF STRONG SCINTILLATION ON SPACE BASED RADAR DESIGN - NONCOHERENT DETECTION	5. TYPE OF REPORT & PERIOD COVERED: Technical Report
	6. PERFORMING ORG. REPORT NUMBER: MRC-R-788
7. AUTHOR(s): Dennis L. Knepp, Roger A. Dana	8. CONTRACT OR GRANT NUMBER(s): DNA 001-83-C-0021
9. PERFORMING ORGANIZATION NAME AND ADDRESS: Mission Research Corporation, P.O. Drawer 719, Santa Barbara, California 93102	10. PROGRAM ELEMENT, PROJECT, TASK AREA & WORK UNIT NUMBERS: Task S99QMXBA-00001
11. CONTROLLING OFFICE NAME AND ADDRESS: Director, Defense Nuclear Agency, Washington, DC 20305	12. REPORT DATE: 1 November 1983
	13. NUMBER OF PAGES: 56
14. MONITORING AGENCY NAME & ADDRESS (if different from Controlling Office)	15. SECURITY CLASS (of this report): UNCLASSIFIED
	15a. DECLASSIFICATION/DOWNGRADING SCHEDULE: N/A since UNCLASSIFIED

16. DISTRIBUTION STATEMENT (of this Report)

Approved for public release, distribution is unlimited.

17. DISTRIBUTION STATEMENT (of the abstract entered in Block 20, if different from Report)

18. SUPPLEMENTARY NOTES

This work was sponsored by the Defense Nuclear Agency under RDT&E RMSS Code B322083466 S99QMXBA00001 H2590D.

19. KEY WORDS (Continue on reverse side if necessary and identify by block number)

Space Based Radar	Fading
Scintillation	Noncoherent Detection
Nuclear Effects	Coherent Detection
Probability of Detection	Rayleigh Fading

20. ABSTRACT (Continue on reverse side if necessary and identify by block number)

Electromagnetic signals which propagate through strongly disturbed regions of the ionosphere can experience scattering which can cause appreciable amplitude, phase and angle-of-arrival fluctuations. This report considers the performance of a space based radar (SBR) that must operate through a highly disturbed propagation environment such as might occur during a barium release or after a high altitude nuclear detonation. A brief summary of the propagation channel characteristics is given in

DD FORM 1 JAN 73 1473 EDITION OF 1 NOV 65 IS OBSOLETE

UNCLASSIFIED

SECURITY CLASSIFICATION OF THIS PAGE (When Data Entered)

20. ABSTRACT (Continued)

terms of quantities that are important to SBR design issues. Previous results for coherent detection performance are summarized and new results are given showing the effect of noncoherent integration on target detection performance. Both coherent and noncoherent detection performance can be seriously affected in a scintillation environment if scintillation is not considered in the radar design.

TABLE OF CONTENTS

LIST OF ILLUSTRATIONS

LIST OF ILLUSTRATIONS (concluded)

TABLE

SECTION 1
INTRODUCTION

Electron density irregularities in the ionosphere can produce random variations in the amplitude and phase of a propagating wave, even at frequencies in the GHz range (Pope and Fritz, 1971; Skinner et al., 1971; Taur, 1976: Fremouw et al., 1978). These rapid variations in signal amplitude, phase, and angle-of-arrival are called scintillations and are often observed over satellite communication links through the ambient ionosphere at VHF and UHF. Strong scintillation is occasionally observed at frequencies as high as L-band. Since even small fluctuations in received power can cause degraded system performance, the effect of scintillation must be considered in the design of a space based radar (SBR) which must operate through an ionospheric channel.

Worst case or Rayleigh amplitude scintillation is likely to occur if the ionosphere is highly disturbed, as for example by high altitude nuclear explosions (Arendt and Soicher, 1964; King and Fleming, 1980) or by chemical releases (Davis et al., 1974; Wolcott et al., 1978). Increased electron concentrations and the irregular structure of the ionization can lead to intense Rayleigh signal scintillation at frequencies as high as the 7-8 GHz SHF band (Knepp, 1977). Consequently, the effects of scintillation are important to any UHF through SHF radar system that must operate through an ionospheric channel and that may have to operate in highly disturbed environments.

In an earlier work (Dana and Knepp, 1983), the impact of a severely disturbed propagation channel on the coherent detection performance of a space based radar was investigated. It was shown that disturbed propagation environments characterized by Rayleigh fading create additional design issues that do not occur for SBR operation in an ambient, undisturbed propagation channel. This report is a continuation of the earlier work that considered the detection performance of an SBR which utilizes coherent processing within a dwell. Here, detection performance is obtained for SBR's that perform noncoherent integration of the amplitudes from multiple dwells that form a radar scan.

SECTION 2
RECEIVED SIGNAL DESCRIPTION

In this report, it is assumed that a space based radar (SBR) must operate through a severely disturbed signal propagation channel that is characterized by severe, Rayleigh fading over a one-way propagation path. By one-way Rayleigh fading is meant that, if a constant signal is transmitted over the channel, then the first order amplitude statistics of the signal received at the channel output are characterized by a Rayleigh probability density function. Rayleigh statistics are worst case for propagation of electromagnetic signals over a wide frequency range in many different kinds of random media including laser propagation in turbulent air (Fante, 1975), and VHF propagation through the ionosphere (Fremouw et al., 1978) and through striations composed of barium ions (Marshall, 1982). In a propagation channel disturbed by a high altitude nuclear detonation, large portions of the signal environment are characterized by Rayleigh fading (Wittwer, 1980; Bogusch et al., 1981).

RECEIVED SIGNAL FIRST-ORDER STATISTICS

In fading conditions it is convenient to write the total received signal, S_r, as

$$S_r = S_0[\sigma/\langle\sigma\rangle]S \qquad (1)$$

The received signal is written as the product of three factors: S_0, the mean signal that would be received from a point target (including the effects of transmitter power, range, frequency, etc.); S, the fractional

change in the signal due to variations caused by the propagation channel; and σ, the change in the signal caused by target fluctuations. The factor S_o contains the mean signal level, therefore $\langle S \rangle$ can be set to unity. Since the mean signal level has no statistical variation, the received signal fluctuations may then be expressed as the product of two terms, the first representing the effect of the target variations and the second representing the effect of signal scintillation.

Target Statistics

In this report, it is assumed that the target cross section fluctuations can be described by either Swerling 1 or by Swerling 2 statistics. In both cases the radar cross section has an exponential probability distribution (or equivalently, a Rayleigh amplitude probability distribution.) Swerling 1 statistics apply to the case that the cross section remains constant over an entire scan (a scan is comprised of one or more coherent dwells or pulse-trains) of the target. Swerling 2 statistics apply to the case that the target radar cross section varies independently from dwell-to-dwell but is constant for all the pulses that comprise a coherent dwell. These terms describing the transmitted radar signal will be clarified later. In either case, the probability density function that describes the target cross section variation is given by the expression

$$p(\sigma) = \frac{1}{\langle\sigma\rangle} \exp(-\sigma/\langle\sigma\rangle) \qquad (2)$$

where $\langle\sigma\rangle$ is the mean value. Equation 2 fully describes the first-order statistics of the target cross section. To completely characterize the first-order statistics of the signal at the radar receiver, one additionally requires the statistics of the signal fluctuations caused by propagation through a disturbed channel.

Propagation Channel Statistics

In the case of satellite communications (SATCOM), the one-way propagation path is often the only case of interest. In the case of an SBR, there are three possible propagation geometries that are potentially important.

One-Way Fading. Under bistatic operation, the radar transmitter and receiver are located separately and thus there may be two independent propagation paths, one from the transmitter to the target and the second from the target to the receiver. For the case that one of these two paths is free space (undisturbed by fading) and the other is severely disturbed, the received signal power is characterized by a Rayleigh probability density function. This one-way fading case is identical to the characterization of a severely disturbed SATCOM channel. For this case, the probability density function of the fluctuations of the power caused by the disturbed propagation channel takes the form

$$p_1(S) = \frac{1}{\langle S \rangle} \exp\{-S/\langle S \rangle\} \qquad (3)$$

where $\langle S \rangle$ is the mean value.

Bistatic SBR Geometry. By the bistatic SBR geometry here is meant the case that the transmitter and receiver are located aboard separate satellites so that the signal travels through two independent one-way propagation channels both of which are severely disturbed by scintillation effects. In this case, the received power is simply the product of the power resulting from each independent one-way propagation path. The probability density function of the product of two independent exponential distributions is easily calculated as (Papoulis, 1965)

$$p_b(S) = \frac{2}{\langle S \rangle} K_o\left(2\sqrt{S/\langle S \rangle}\right) \qquad (4)$$

where K_o is the modified Bessel function (Abramowitz and Stegun, 1965). $\langle S \rangle$ is again the mean received power.

Monostatic SBR Geometry. For the case of monostatic SBR operation, the transmitter and receiver are colocated so that the signal propagates twice over the same path passing through identical irregularities. In this case, the received voltage is proportional to the square of the voltage after one-way propagation. The received power is similarly proportional to the square of the received power after one-way propagation. The probability distribution function of the received power then may be obtained from Equation 3 using the transformation S (monostatic) = S^2 (one-way) with the result

$$p_m(S) = \frac{1}{\sqrt{2S\langle S \rangle}} \exp\left\{-\sqrt{2S\langle S \rangle}\right\} \qquad (5)$$

where $\langle S \rangle$ is the mean value.

Cumulative Distribution of Channel and Target Fluctuations

The effects of fluctuations in the propagation channel and target cross section fluctuations can be combined in the form of a probability distribution function that represents the product of two independent random variables. The cumulative distribution function of the received power is given for the three cases under consideration as

$$P_1(S_r) = 1 - 2\sqrt{S_r/S_0}\, K_1(2\sqrt{S_r/S_0}) \qquad (6a)$$

$$P_b(S_r) = 1 - \int_0^\infty u\, K_0(u) \exp\{-4S_r/(u^2 S_0)\}\, du \qquad (6b)$$

$$P_m(S_r) = 1 - \int_0^\infty \exp\{-u - 2S_r/(u^2 S_0)\}\, du \qquad (6c)$$

where the subscripts 1, b, and m refer to the one-way propagation path, the bistatic case, and the monostatic radar case, respectively. K_0 and K_1 are the modified Bessel functions (Abramowitz and Stegun, 1965) and S_0 is the mean received power.

In the absence of scintillation, the received power is that from the Swerling 1 target alone and the cumulative probability distribution function of the received power is the integral of Equation 2

$$P_{\text{no scint}}(S_r) = 1 - \exp\{-S_r/S_0\} \qquad (7)$$

Figure 1 is a plot on probability paper of the cumulative probability distributions for the four different situations considered. The curve denoted "no fading," is simply a plot of Equation 7 and describes the situation of a Swerling 1 target that is usually considered in the design phase to determine the radar power requirements. Since this curve also applies to a Rayleigh amplitude distribution, it is valid for the case of propagation of a constant signal through strong irregularities as would occur for transionospheric satellite communications.

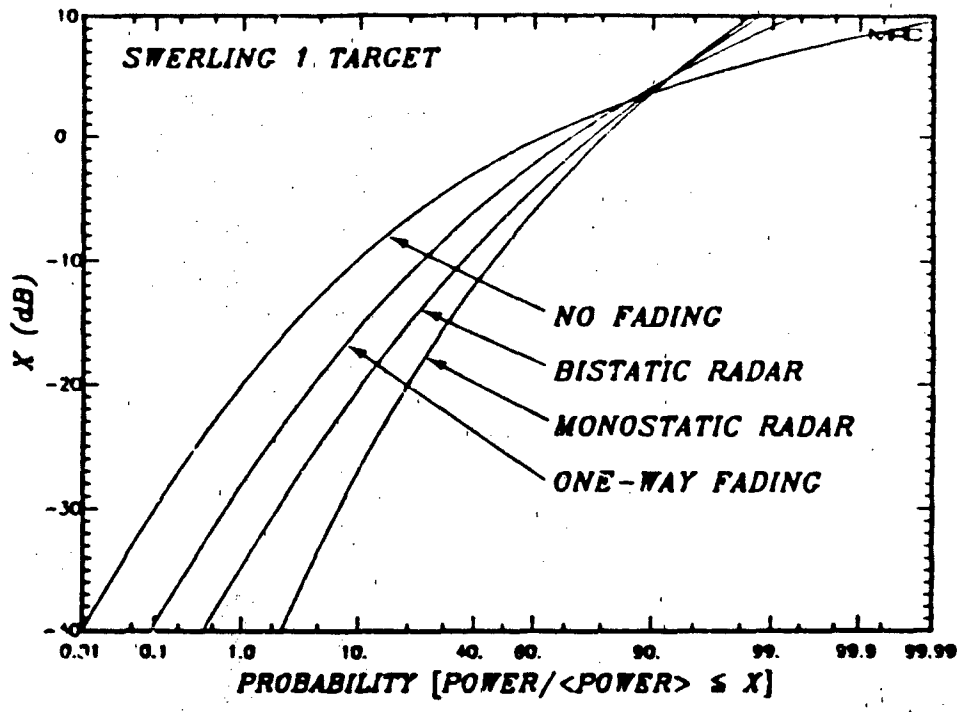

Figure 1. Cumulative probability distribution function of the received power for a Swerling 1 target and various propagation geometries.

It is apparent that the effect of scintillation is to increase the probability of deep fades beyond that expected for a Swerling 1 target alone. For example, a Swerling 1 target, with no propagation fading, gives a probability of 10^{-4} for fades of 40 dB or greater. For monostatic operation, the probability of a fade of 40 dB or greater is 0.02. It will be shown that this increased chance of deep fading caused by the disturbed transionospheric channel causes degradation of target detection performance of an SBR.

RECEIVED SIGNAL SECOND-ORDER STATISTICS

The above discussion fully describes the first-order or amplitude statistics to be expected after propagation of a radar signal through a severely disturbed channel. Note that this description is valid only

for the worst-case situation where Rayleigh statistics characterize the one-way propagation channel. Many other statistical descriptions are possible for the received signal in less severely disturbed environments. However, the signal description here leads to the most severe effects on SBR performance.

The second-order fading statistics are specified by the correlation function of the received complex voltage. For the case of one-way propagation of an initially constant amplitude signal through a severely disturbed ionospheric channel, the autocorrelation function of the received voltage is given as the two-position, two-frequency mutual coherence function (Knepp, 1983).

Signal Decorrelation Time

For a K^{-4} in situ power spectrum of three-dimensional ionization irregularities between outer scale L_0 and inner scale ℓ_i, the decorrelation time is (Knepp, 1983)

$$\tau_1 = \sqrt{2}\, L_0/\ell n(L_0/\ell_i)\sigma_\phi v_L \qquad (8)$$

where

v_L = the velocity of the line-of-sight through the center of the ionized layer

$\sigma_\phi^2 = 2(r_e\lambda)^2 L_0 L \overline{\Delta N_e^2}$ rad^2

λ = RF wavelength

r_e = classical electron radius (2.82×10^{-15} m)

L = thickness of ionized layer

$\overline{\Delta N_e^2}$ = variance of electron density irregularities

The signal one-way decorrelation time τ_1 is an inverse measure of the fading rate or fading bandwidth. Large values of τ_1 correspond to slow fading conditions and small values correspond to fast or rapid fading.

For the bistatic SBR propagation geometry, the decorrelation time of the received signal is related to the decorrelation time for each of the individual propagation channels according to the relationship (Dana and Knepp, 1983)

$$\tau_o = \left| \frac{\tau_1^2 \tau_2^2}{\tau_1^2 + \tau_2^2} \right|^{1/2} \tag{9}$$

where τ_1 and τ_2 are the decorrelation times of the two individual one-way propagation paths.

For the monostatic SBR geometry, the two channels are coincident (by the principal of reciprocity) and the decorrelation time is

$$\tau_0 = \tau_1/\sqrt{2} \tag{10}$$

where τ_1 is the decorrelation time of the one-way propagation path.

For worst case Rayleigh fading the correlation function of the received complex voltage always has the Gaussian form

$$\langle E^*(t+\tau)E(t)\rangle = \exp\{-\tau^2/\tau_o^2\} \tag{11}$$

for any of the three possible geometries (Dana and Knepp, 1983). In the following, the signal decorrelation time will always be denoted by the symbol τ_0 independent of the various propagation paths. The actual value of τ_0 is, of course, a function of the geometry as well as the irregularity structure of the ionospheric propagation channel.

In this report it is assumed that τ_0 is large with respect to the duration of the transmitted pulse so that the received signal is coherent during this brief time period that is typically of the order of several tens of microseconds.

Channel Coherence Bandwidth

The channel coherence bandwidth is a measure of the maximum bandwidth available in the propagation channel over which it is possible to transmit a signal without imposition of undesired pulse distortion. That is, in a fading environment, signal spectral components separated by less than the coherence bandwidth exhibit perfectly correlated fluctuations. If the signal spectral components are separated by an amount greater than the coherence bandwidth, then different spectral components will undergo uncorrelated fading. This distortion in the received signal spectrum causes the received time domain signal to display undesired time sidelobes. On the other hand, a propagating pulse remains undistorted as long as the maximum instantaneous signal bandwidth is less than the coherence bandwidth. This is often the case for frequency hopped radar systems. However, frequency hopped signals that are separated in frequency by an amount exceeding the coherence bandwidth will experience independent fading.

For a K^{-4} in situ power spectrum of three-dimensional ionization irregularities the coherence bandwidth is given by

$$\omega_{coh} = \frac{\sqrt{2}\,\pi^2 c(z_t+z_r)L_o}{r_e^2\lambda^4 \ell n(L_o/\ell_i) z_t z_r L \overline{\Delta N_e^2}} \qquad (12)$$

for the case of a monostatic SBR propagation geometry. This value is smaller than the coherence bandwidth for one-way propagation by a factor of $1/\sqrt{2}$ (Knepp, 1982). In this expression

c = velocity of light in vacuum

z_t = distance from the transmitter to the center of the ionized layer

z_r = distance from the target to the center of the ionized layer

$z_t + z_r$ = total one-way propagation distance

For the case of the bistatic SBR propagation channel, the coherence bandwidth is related to the coherence bandwidth of each of the one-way propagation paths by

$$\omega_{coh} = \left\{ \frac{\omega_{coh1}^2 \, \omega_{coh2}^2}{\omega_{coh1}^2 + \omega_{coh2}^2} \right\}^{1/2} \tag{13}$$

In this report, it is assumed that the channel coherence bandwidth is sufficiently large compared to the radar pulse bandwidth so that no time domain distortion of the received pulse occurs. However, variations in the coherence bandwidth with respect to the frequency hopping bandwidth of a jam resistant frequency agile radar are considered here. It will be shown that such variations affect the probability of target detection when dwells transmitted at different radar frequencies are noncoherently combined.

SECTION 3
RADAR SYSTEM CHARACTERISTICS

In this report, it is assumed that an SBR operates through a disturbed ionospheric channel to detect and track targets near the earth's surface. Thus, relative to a ground based radar with similar functions, an SBR has several limitations. First, targets are detected and tracked at very long ranges Second, available onboard transmitter power is relatively low.

These two points imply low received signal-to-noise ratio per pulse and therefore require long integration times. However, the cross section of a moving target remains constant or coherent for only a few tens of milliseconds because of target mc ion and resulting constructive and destructive interference between many scattering centers. Hence, during a radar scan, the total energy transmitted at a target is divided into a number of dwells (also referred to as bursts). Each dwell consists of some number, n, of pulses transmitted at some radar frequency, which are coherently integrated upon reception. The radar frequency is changed between dwells as a form of jamming protection and to assure independent samples of the target cross section. The detected amplitudes of all the dwells which form the total radar target scan are then noncoherently combined in a postdetection integration process.

Figure 2 shows a simplified block diagram of a generic SBR receiver. The complex input signal contains amplitude, phase and doppler information from target, clutter, and thermal noise sources. The weighted

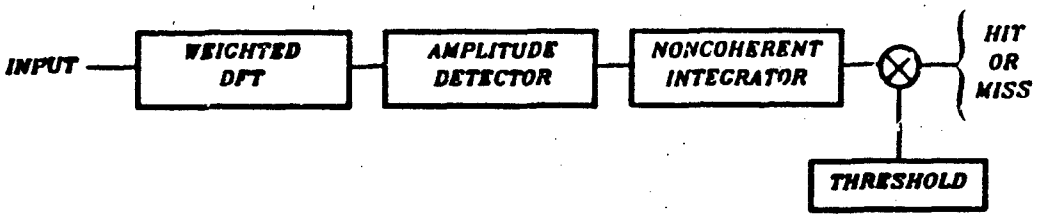

Figure 2. Block diagram of generic SBR receiver.

discrete Fourier transform (DFT) simultaneously acts as a coherent integrator and as a clutter rejection filter. After the amplitude from a single dwell is obtained from the amplitude detector, the radar frequency is changed and several more dwells transmitted at different frequencies. Any number of these independent samples may then be noncoherently combined and the resulting amplitude compared to a threshold and a "hit" or "miss" declared. For the sake of simplicity in subsequent calculations, it is assumed that the target doppler is zero and that no clutter rejection filtering is applied.

SECTION 4
PROBABILITY OF DETECTION

In this report, SBR target detection performance is summarized for the case of one dwell per scan for slow and fast fading. These results are described in detail in a previous report (Dana and Knepp, 1983). The case of multiple dwells per scan is then considered in detail and results are presented for the situation in which a frequency selective propagation environment acts to decorrelate the propagation disturbance from dwell-to-dwell.

PROPAGATION EFFECTS ON COHERENT INTEGRATION

Since an SBR will be required to operate over a wide range of fading rates relative to the coherent processing time, a distinction can be made between slow and fast fading that is an invaluable aid in understanding the effects of scintillation on receiver performance.

Slow Fading

In slow fading conditions, the duration of signal fluctuations is very long compared to the coherent processing (or dwell) time. Hence the signal amplitude and phase are relatively constant over the receiver coherent integration time which, in the expanded receiver model of Figure 3, is the time to integrate n pulses. In this case only dwell-to-dwell or scan-to-scan signal amplitude fluctuations affect SBR target detection performance. Therefore, the effect of slow fading on target detection performance may be determined solely on the basis of the first-order signal amplitude statistics expressed by Equations 3-5.

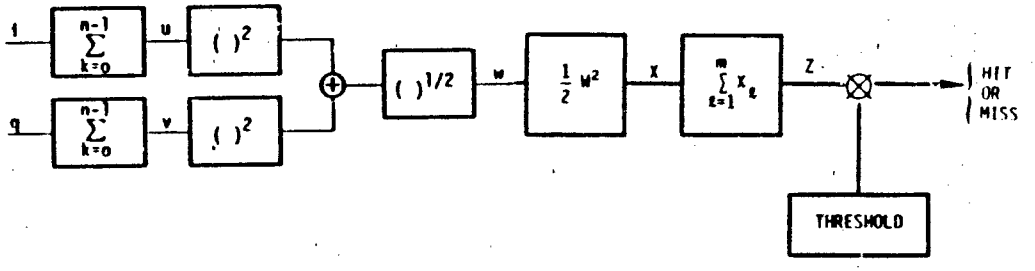

Figure 3. Expanded block diagram of SBR receiver.

In slow fading, the amplitude output from the coherent integration shown in Figure 3, $w = (u^2+v^2)^{1/2}$, has the well known Rician probability density function (Dana and Knepp, 1983)

$$p(w|a) = \frac{w}{n\sigma_N^2} \exp\{-(w^2+n^2a^2)/2n\sigma_N^2\}\, I_0(wa/\sigma_N^2) \qquad (14)$$

where a is the target amplitude per pulse, n is the number of coherently integrated pulses, $2\sigma_N^2$ is the total noise power per pulse, (σ_N^2 is the noise power per pulse in each of the quadrature channels), and I_0 is the modified Bessel function. Equation 14 assumes that the amplitude a does not change during the coherent dwell.

Now consider the effect of target cross section fluctuations while, for the moment, allowing no fluctuations due to the turbulent propagation environment. Thus assume that S, the propagation contribution to the power as given by Equation 1, is constant. If the target cross section has a Swerling 1 distribution, as given by Equation 2, the target amplitude probability density function is then

$$p(a|S) = 2a \exp\{-a^2/SS_0\}/SS_0 \qquad (15)$$

for a fixed value of S. Now the probability density function for the envelope w may be calculated as

$$p(w|S) = \int_0^\infty p(w|a)p(a|S)da \tag{16}$$

or simply

$$p(w|S) = \frac{w}{n\sigma_N^2(1+nSS_0/2\sigma_N^2)} \exp\left\{-\frac{w^2}{2n\sigma_N^2(1+nSS_0/2\sigma_N^2)}\right\} \tag{17}$$

In the single dwell per scan case, it is sufficient to consider only the amplitude w. After detection, the signal amplitude is compared to a threshold value and a hit or miss is declared. The threshold value t is set on the basis of the noise alone to achieve a desired probability of a false alarm P_{fa} given by

$$P_{fa} = \int_t^\infty p(w|S_0=0)dw = \exp\{-t^2/2n\sigma_N^2\} \tag{18}$$

The probability that the signal will be detected for a given value of S is the same as the probability that the signal amplitude w will exceed the threshold. Therefore

$$P_d(S) = \int_t^\infty p(w|S)dw = P_{fa}^{\frac{1}{1+\langle SNR\rangle S}} \tag{19}$$

where $\langle SNR\rangle = nS_0/2\sigma_N^2$ is the mean signal-to-noise ratio per dwell. Equation 19 gives the well known relationship between false alarm probability and probability of detection for a Swerling 1 target with mean power S_0 for a fixed propagation condition or a fixed value of S.

To obtain the probability of detection for the case of a Swerling 1 target combined with propagation through strongly turbulent ionization, it is convenient to calculate the probability of detection according to Equation 19 for a given value of power S and then to average over the distribution of power. The probability of detection is then written as

$$P_d = \int_0^\infty P_{fa}^{\frac{1}{1+\langle SNR \rangle S}} p_{prop}(S)dS \qquad (20)$$

where $p_{prop}(S)$ is the power distribution after single or multiple trans-ionospheric propagation and is given by Equation 3, 4, or 5, whichever is appropriate to the actual geometry, with <S> set equal to unity.

The average probability of detection for a Swerling 1 target with no scintillation and with one-way, bistatic and monostatic scintillation geometries is shown in Figure 4 for a false alarm probability P_{fa} of 10^{-6}, typical of a modern search radar. For the one-way, bistatic, and monostatic scintillation geometries the results are obtained using numerical integration techniques. For the Swerling 1 target with no scintillation, Equation 19 is plotted with S=1. As was to be expected from the cumulative probability distribution statistics, the monostatic case has the greatest detection sensitivity loss and the bistatic case has somewhat less loss. Relative to the optimum detection curve with no propagation

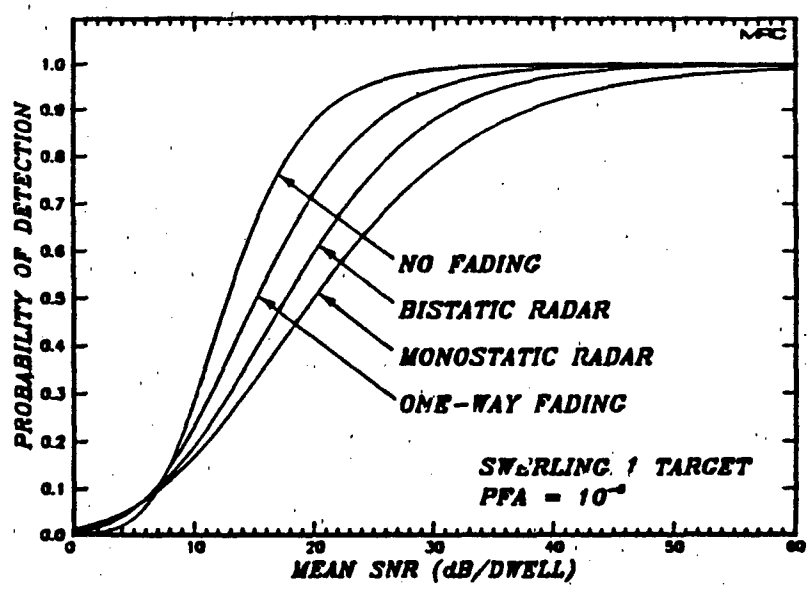

Figure 4. Probability of detection as a function of SNR for slow fading conditions.

fading, at a 0.7 probability of detection value, the detection sensitivity losses are 4 dB with one-way fading, 7 dB with bistatic fading, and 11 dB with monostatic fading. Thus, it appears that, during severe slow fading, a gain of 4 dB is possible by using bistatic operation instead of monostatic operation. This 4 dB gain in detection sensitivity may not be realizable when the differences in monostatic and bistatic geometry and radar cross section are taken into account.

Fast Fading

In fast fading conditions, the signal decorrelation time is less than the SBR coherent integration time and the effectiveness of coherent processing is reduced. Equivalently, the signal bandwidth is spread beyond the receiver bandwidth so that signal energy is lost. This loss is caused by destructive interference of radar pulses which are uncorrelated in amplitude and phase with preceding and following pulses during the coherent integration time. This fast fading imposes additional loss in detection sensitivity beyond that imposed in slow scintillation.

Under fast fading conditions, the analytic approach used above is no longer generally sufficient since the received signal is decorrelated during the duration of a dwell. For the bistatic and monostatic SBR geometry, it is necessary to generate Monte Carlo realizations of the received voltage which possess the required first- and second-order statistical description.

To compute the probability of detection, many independent realizations of the received quadrature voltages are generated, each realization is then numerically integrated and a pseudo-random sample of the integrated noise voltage is added. At this point the integrated voltages are amplitude detected. This signal-plus-noise output amplitude is then compared to the threshold and a hit or a miss is declared. The detection process is repeated many times to obtain probability of detection statistics as a function of signal decorrelation time.

Figure 5 shows probability of detection versus the mean signal-to-noise ratio $nS_0/2\sigma_N^2$ in dB per dwell, for monostatic SBR operation with a probability of false alarm of 10^{-6}. In the figure, the probability of detection is shown for a Swerling 1 target with no fading, and for a Swerling 1 target with slow fading. These curves are taken directly from Figure 4. The simulation results for fast fading are shown as points which are connected by smooth dashed curves and denoted by values of τ_0/T_{Ci}, the ratio of decorrelation time to coherent integration time. To obtain these results, each dwell is formed from 400 pulses. The 95 percent confidence interval is shown about one of the simulation results.

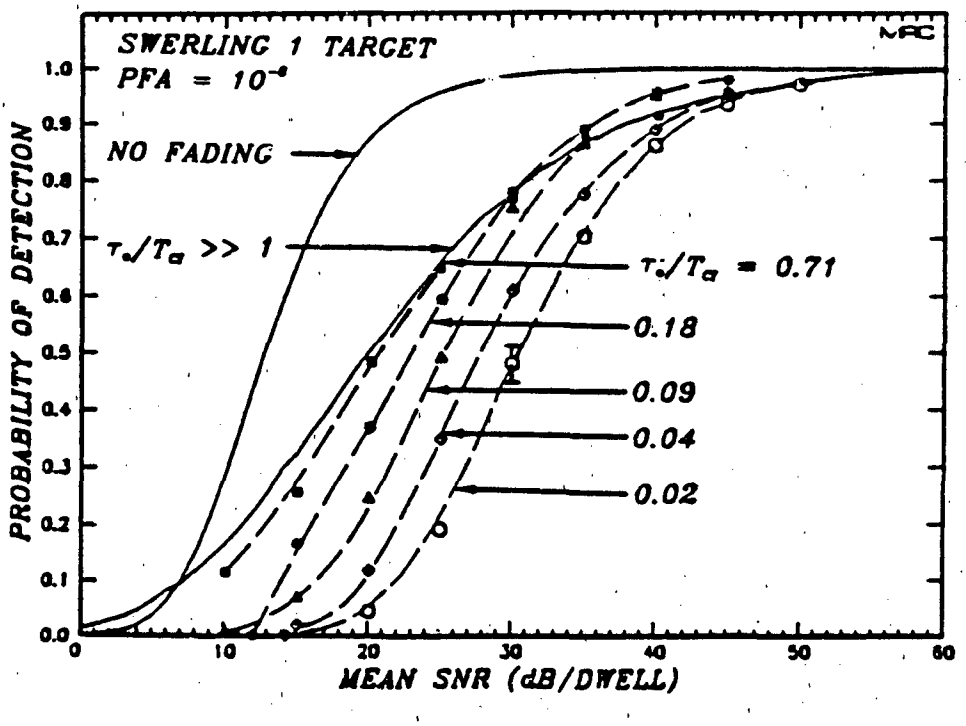

Figure 5. Probability of detection for monostatic space based radar.

Figure 5 shows that fast fading causes considerable additional loss in detection sensitivity. For a value of about 0.02 for the ratio of signal decorrelation time to SBR coherent integration time, the additional loss is about 8 dB relative to the slow fading ($\tau_0 \to \infty$) limit at a P_d

value of 0.7. As the decorrelation time increases to approach the coherent integration time, the P_d values approach the slow fading limit as expected. The results for fast fading in this figure show that the slow fading limit for P_d is exceeded by the curves for values of τ_0/T_{ci} of 0.09 and 0.18 for mean signal-to-noise ratios above 30 dB. This behavior is the result of two competing effects. As τ_0/T_{ci} decreases the efficiency of the coherent integration process is degraded. However, as τ_0/T_{ci} decreases, the number of independent samples of the received signal increases, thereby changing the statistics of the output of the coherent integrator. For monostatic operation, with the very severe input amplitude statistics, the change towards more favorable statistics gives a very slight gain in detection performance over a small range of τ_0/T_{ci} values.

PROPAGATION EFFECTS ON NONCOHERENT INTEGRATION

In this section, the effects of fading are determined as it impacts the detection performance of an SBR that utilizes noncoherent integration of many dwells that comprise a scan. Slow fading conditions are assumed in the remainder of this report so that the signal decorrelation time (due to fading) is large with respect to the duration of all the dwells of an entire scan. Thus, there is no loss due to pulse-to-pulse decorrelation during the coherent integration process shown in Figure 3.

Furthermore, this slow fading assumption introduces the feature that the propagation effects are controlled by the relationship between the radar hopping bandwidth and the channel coherence bandwidth. For example, if the coherence bandwidth is much larger than the hopping bandwidth, changes in the radar frequency from dwell-to-dwell introduce no changes in the observed scintillation during that scan. Conversely, if the radar hopping bandwidth is large with respect to the channel bandwidth, the voltage component due to scintillation changes from dwell-to-dwell providing statistical variation and giving improved detection performance.

First, a comparison of detection probability is given for ambient environments with no fading for the case of Swerling 1 and 2 targets. Probability of detection is calculated for the combination of the coherent integration of the voltage from n pulses during a dwell and the noncoherent integration of the amplitudes from m dwells during a scan. From these results, it will be seen that there is an optimum number greater than unity of dwells per scan when the energy allocated for target detection is fixed (i.e., constant m × n) and when the radar transmission frequency is changed from dwell-to-dwell. Although these results were first derived by Swerling (1960) many years ago, they are cast here in a form that includes both coherent and noncoherent integration.

Then three cases are examined. First, the case that the propagation channel bandwidth is very large with respect to the radar hopping bandwidth (ω_{hop}) is considered. In this case the received signal contribution from the fading channel remains constant during the entire scan. Second, results are presented for the case that the propagation channel bandwidth is small with respect to the radar hopping bandwidth. In this case the contribution to the received signal from scintillation effects is independent from dwell-to-dwell. Third, the intermediate situation where the channel fluctuations are correlated from dwell-to-dwell is considered. In all three cases here, the SBR frequency is changing between dwells, so that a Swerling 2 target model is appropriate.

In the following, it is shown that there is a significant gain in SBR detection performance for the case that the propagation scintillation effects from dwell-to-dwell are totally or partially decorrelated.

Undisturbed Environment

Swerling 1 Target. For the case of a Swerling 1 target and no propagation fading, the radar cross section, and therefore the target amplitude, is constant for all the dwells of a scan. For a fixed target

amplitude, the probability density function of the output of the coherent integrator is given by Equation 14. The probability density function of x (see Figure 3) is then the Rician power distribution

$$p(x|A) = \frac{1}{n\sigma_N^2} \exp[-(x+n^2A/2)/n\sigma_N^2] I_0(\sqrt{2Ax}/\sigma_N^2) \qquad (21)$$

where $A = a^2$ is the constant target power per pulse.

The distribution of the output amplitude from the sum of m amplitudes each with the probability density function of Equation 21 is obtained by noting that the probability distribution of the sum of independent random variables has as its characteristic function the product of the characteristic functions of the individual random variables. The amplitudes x_ℓ ($\ell = 1,2,\ldots,m$) are independent because the noise components of the amplitudes are independent. The target power A represents a constant component which is common to all of the terms.

The characteristic function is the Fourier transform of $p(x|A)$ so that

$$C_1(q|A) = \int_0^\infty e^{-qx}\, p(x|A)dx \qquad (22)$$

where q is an imaginary transform variable and where the subscript 1 refers to the fact that $C_1(q|A)$ is the characteristic function of one of the amplitudes in the noncoherent integration. Performance of the indicated integration (Gradshteyn and Ryzhik, 1965) gives

$$C_1(q|A) = \frac{\exp\{-n^2Aq/[2(n\sigma_N^2q+1)]\}}{n\sigma_N^2q+1} \qquad (23)$$

Since the amplitude z is the sum of m independent values of x, the characteristic function of $p(z|A)$, the probability density function of z for a given target power, is then

$$C_m(q|A) = [C_1(q|A)]^m$$

$$= \frac{\exp\{-mn^2Aq/[2(n\sigma_N^2q+1)]\}}{(n\sigma_N^2q+1)^m} \qquad (24)$$

The probability density function of z for a given value of A, $p(z|A)$, is the inverse Fourier transform of $C_m(q|A)$. This can then be averaged over the scan-to-scan distribution of A to obtain $p(z)$ for a Swerling 1 target. Noting that the order of integration is unimportant, it is convenient to average $C_m(q|A)$ over the distribution of A and then take the inverse Fourier transform to obtain $p(z)$. For a Swerling 1 target, the probability density function of the received power is

$$p(A) = \exp(-A/S_0)/S_0 \qquad (25)$$

where, again, S_0 is the mean received power per pulse. The average of $C_m(q|A)$ gives

$$C_m(q) = \int_0^\infty C_m(q|A)p(A)dA$$

$$= \frac{1}{(n\sigma_N^2q+1)^{m-1}[1+n\sigma_N^2q[1+mnS_0/(2\sigma_N^2)]]} \qquad (26)$$

The inverse Fourier transform (Campbell and Foster, 1948) of $C_m(q)$ gives the probability density function of z as a function of the mean signal-to-noise ratio as

$$p(z) = \left[\frac{1+m<SNR>}{m<SNR>}\right]^{m-1} \frac{\exp\{-z/[n\sigma_N^2(1+m<SNR>)]\}}{n\sigma_N^2(1+m<SNR>)}$$

$$\times \frac{\gamma\{m-1, m<SNR>z/[n\sigma_N^2(1+m<SNR>)]\}}{\Gamma(m-1)} \qquad (27)$$

where γ is the incomplete gamma function, and $\Gamma(m-1)$ is the gamma function (Abramowitz and Stegun, 1965). For later reference note that $\Gamma(a,x) + \gamma(a,x) = \Gamma(a)$ where $\Gamma(a,x)$ is also referred to as the incomplete gamma function. The factor $\langle SNR \rangle$ is the mean signal-to-noise ratio per dwell defined in connection with Equation 19.

Swerling 2 Target. In the case of a Swerling 2 target, the radar cross section is independent from dwell-to-dwell, and the probability density function of the amplitude w at the output of the coherent integrator is given by Equation 17 for a constant value of S, the contribution of propagation fading to the received power. Note that Equation 17 already includes the contribution of the Swerling 2 target. The probability density function of x then has the exponential form

$$p(x|S) = \frac{\exp\{-x/[n\sigma_N^2(1+S\langle SNR\rangle)]\}}{n\sigma_N^2(1+S\langle SNR\rangle)} \qquad (28)$$

where $\langle SNR \rangle$ is the mean signal-to-noise ratio per dwell. Noting that the sum of m independent exponentially distributed random variables is a χ^2 variable with $2m$ degrees of freedom, the probability density function of z for a fixed value of S, the contribution from fading, is

$$p(z|S) = \frac{\{z/[n\sigma_N^2(1+S\langle SNR\rangle)]\}^{m-1} \exp\{-z/[n\sigma_N^2(1+S\langle SNR\rangle)]\}}{n\sigma_N^2(1+S\langle SNR\rangle)\Gamma(m)} \qquad (29)$$

where $\Gamma(m) = (m-1)!$ is the gamma function.

Results. After the noncoherent process is completed, the amplitude z is compared with a threshold and a hit or miss is declared. The threshold is set so that the probability of a hit from noise alone is small (typically 10^{-4} to 10^{-8}). The probability of false alarm is then just the integral of Equation 29 with the target cross section set to zero.

$$P_{fa} = \int_{T}^{\infty} p(z|S=0)dz = \Gamma[m, T/(n\sigma_N^2)]/\Gamma(m) \qquad (30)$$

where $\Gamma(m,x)$ is the incomplete gamma function. It is an easy matter to numerically invert Equation 30 to find $T/n\sigma_N^2$ as a function of the probability of false alarm and the number of dwells per scan, m. Since the noise is independent of target or channel statistics, Equation 30 for the threshold does not depend on the target or channel model.

Once the threshold has been obtained, the probability of detection becomes

$$P_d(S) = \int_{T}^{\infty} p(z|S)dz \qquad (31)$$

which is the probability that an amplitude z of signal plus noise exceeds the threshold for a given value of S, the signal contribution due to fading.

For the case of a Swerling 1 target with no fading, it is necessary to perform the integration given by Equation 31 using Equation 27 as the integrand. After some manipulation the probability of detection is found as

$$P_d = P_{fa} + \left[\frac{1+m\langle SNR\rangle}{m\langle SNR\rangle}\right]^{m-1} \exp\{-T/[n\sigma_N^2(1+m\langle SNR\rangle)]\} \times \frac{\gamma\{m-1, m\langle SNR\rangle T/[n\sigma_N^2(1+m\langle SNR\rangle)]\}}{\Gamma(m-1)} \qquad (32)$$

Since $T/n\sigma_N^2$ is independent of n, the probability of detection depends only on the mean signal-to-noise ratio per dwell, the number of dwells per scan, and the probability of false alarm. Also, it is easy to show that $P_d = P_{fa}$ when <SNR> is zero.

The probability of detection for a Swerling 2 target has the simpler form

$$P_d(S) = \Gamma\{m, T/[n\sigma_N^2(1+S\langle SNR\rangle)]\}/\Gamma(m) \qquad (33)$$

which is again independent of n for a given signal-to-noise ratio per dwell. Equation 33 gives the probability of detection of a Swerling 2 target for a fixed propagation scintillation condition or a fixed value of S. The result for the case of no fading is found by taking S as unity in the equation. The results for the case of propagation scintillation may, in some cases as follows, be obtained from Equation 33 after averaging over the probability distribution function of S.

The probability of detection is shown in Figure 6 for a Swerling 1 target versus the mean signal-to-noise ratio per scan, m<SNR>. The number of dwells noncoherently integrated is 1, 2, 4, 8, or 16. In the absence of target cross section fluctuations from dwell-to-dwell, the signal-to-noise ratio required to achieve a given probability of detection increases as the number of dwells per scan is increased. Thus these results demonstrate the well known result that for a Swerling 1 target or, equivalently, for a radar that does not change transmission frequencies from dwell-to-dwell, the optimum number of dwells per scan is one.

However, when the radar transmission frequency is changed from dwell-to-dwell so that the target cross section fluctuations are described by the Swerling 2 model, the detection curves of Figure 7 are obtained.

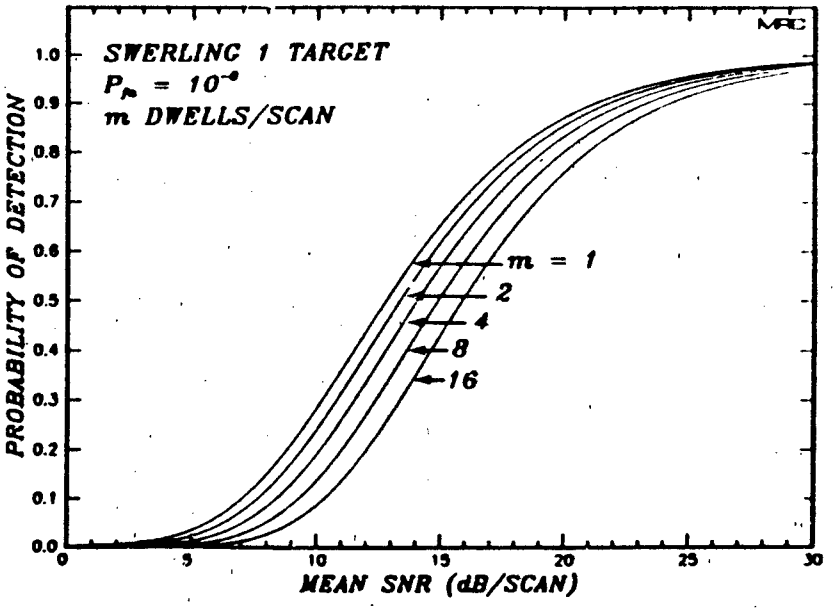

Figure 6. Probability of detecting a Swerling 1 target in an undisturbed propagation environment.

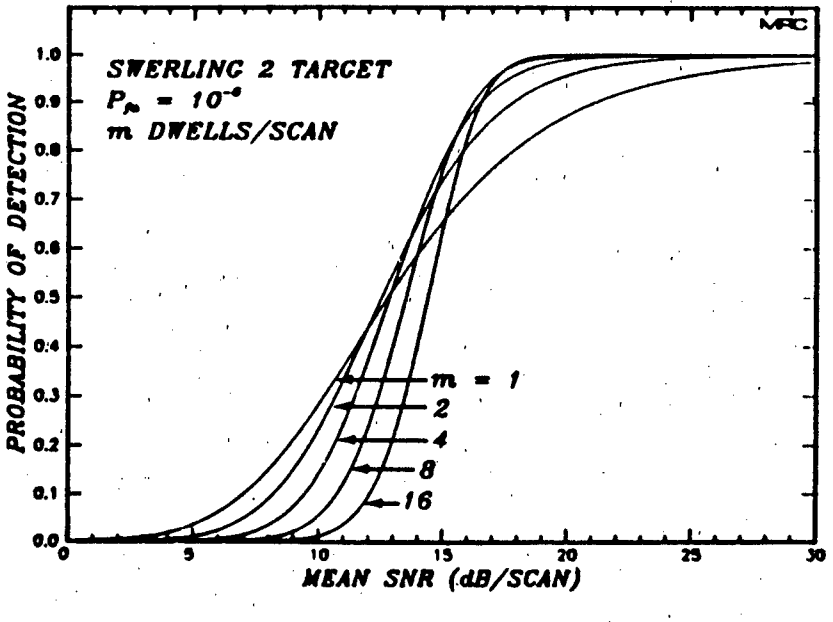

Figure 7. Probability of detecting a Swerling 2 target in an undisturbed propagation environment.

From the figure, for signal-to-noise ratios less than about 15 dB per scan, the number of dwells per scan which minimizes the signal-to-noise ratio required to achieve a given probability of detection depends on the probability of detection. If an SBR could always operate at signal-to-noise ratios above 15 dB per scan, then the optimum number of dwells per scan is the largest number possible. In general, however, it is desirable that the detection performance of the radar degrade as gracefully as possible as the signal-to-noise ratio falls until the point where the probability of detection falls below the minimum (say 50 percent) required to maintain a radar track. At a 50 percent probability of detection, the two dwell per scan case requires a signal-to-noise ratio of only 12.5 dB per scan whereas the 16 dwell per scan case requires 14.5 dB per scan. The optimum number of dwells per scan will therefore be arbitrarily defined by finding the detection curve which, for probabilities of detection above 0.5, minimizes the difference between the signal-to-noise ratio that it requires to achieve a given probability of detection and the minimum signal-to-noise ratio required to achieve that same probability of detection. For the detection curves plotted in Figure 7, the optimum number of dwells per scan is 4.

By comparing Figures 6 and 7, it can be seen that for probabilities of detection greater than about 0.3 and for the number of dwells per scan greater than unity, a Swerling 2 target requires a smaller signal-to-noise ratio to achieve a given probability of detection than does a Swerling 1 target.

The results presented above show that the optimal number of dwells per scan is about 4 when the transmission frequency is changed from dwell-to-dwell. Otherwise, a single dwell per scan is optimal. However, these waveform design considerations are limited by many practical constraints. The maximum duration of a coherent dwell is limited, for example, by the time duration of radar cross section fluctuations caused by

target motion or by other considerations such as the coherence time of the receiver phase reference. On the other hand, the minimum number of pulses per dwell or equivalently the minimum duration of a dwell is limited, for example, by doppler resolution and clutter attenuation requirements. Therefore, it is not possible to choose the number of dwells per scan merely on the basis of target detectability considerations. In addition, an SBR may be required to operate at lower probabilities of detection than ground based radars because of power constraints. Decreasing probability of detection with decreasing signal-to-noise ratio might then drive the waveform design to 2 or 3 dwells per scan.

Effects of Fading on Noncoherent Integration

Now consider the case that the signal decorrelation time is large with respect to the duration of all the dwells that comprise a scan. Under this slow fading assumption, the propagation effects are controlled by the relationship between the SBR hopping bandwidth, ω_{hop}, and the propagation channel coherence bandwidth, ω_{coh}. In the following, the radar frequency is changed for each dwell so that a Swerling 2 target model applies.

Large Channel Coherence Bandwidth. For the case that $\omega_{coh} \gg \omega_{hop}$, the contribution to the received signal due to channel fluctuations is constant during a scan but varies independently from scan-to-scan. Thus, the probability of detection during fading is computed by averaging the probability of detection for constant propagation conditions over the appropriate distribution function describing the propagation channel fluctuations. That is,

$$P_d = \int_0^\infty P_d(S) P_{prop}(S)\, dS \qquad (34)$$

where $P_{prop}(S)$ is the probability density function for one-way, monostatic, or bistatic propagation geometries. In general, it is necessary to evaluate Equation 34 using numerical quadrature techniques.

Small Channel Coherence Bandwidth. If $\omega_{coh} \ll \omega_{hop}$, the contribution to the signal from propagation scintillation is independent from dwell-to-dwell. In this case, the distribution of the amplitude out of the square-law detector (Equation 33) must first be averaged over the dwell-to-dwell distribution of S before the noncoherent integration process can be considered. To the authors' knowledge, this average cannot be obtained in closed form for any of the propagation geometries considered here. It is therefore necessary to use Monte Carlo techniques to obtain the probability of detection.

Here random samples of S are generated from the appropriate distribution and then Equation 28 is used to generate m random samples of the output amplitude from the square-law detector. The amplitudes are noncoherently integrated and compared with the threshold from Equation 30 to declare a hit or a miss. The probability of detection is then estimated as the ratio of the number of hits to the number of trials or scans.

The samples of S, the fading propagation channel contribution to the signal, are generated by noting that for one-way propagation the probability density function of S is exponential:

$$p(S) = e^{-S} \quad . \tag{35}$$

Independent samples of S are then obtained by inverting the equation

$$F(S) = \int_0^S p(S')dS' = 1 - e^{-S} = 1-U \tag{36}$$

where $F(S)$ is the cumulative distribution of S and U is a uniformly distributed random variable on the interval $(0,1]$. For a monostatic SBR geometry, S is the square of the one-way value; for the bistatic SBR geometry, S is the product of two independent one-way values. Hence the values of S are generated in all three SBR geometries as

$$S = \begin{cases} -\ell n\ U & \text{one-way} \\ \frac{1}{2}\ \ell n^2 U & \text{monostatic} \\ \ell n\ U\ \ell n\ U' & \text{bistatic} \end{cases} \tag{37}$$

where U and U' are independent variates with uniform distributions. The mean value of S is unity in each case.

For a given value of S generated from Equation 37, the samples of the amplitude at the output of the square-law detector are obtained by inverting the cumulative distribution of amplitude. In this case the cumulative distribution function of the output amplitude x is given as the integral of Equation 28 with respect to x. Random samples of the amplitude may then be obtained in the same manner as above from the expression

$$x/n\sigma_N^2 = -(1 + \langle SNR \rangle S)\ \ell n\ U'' \tag{38}$$

where $\langle SNR \rangle$ is the input value of the mean signal-to-noise ratio per dwell and where U'' is another uniformly distributed random variable.

The noncoherently integrated amplitude may then be written as

$$z/n\sigma_N^2 = -\sum_{i=1}^{m} (1 + \langle SNR \rangle S_i)\ \ell n\ U_i \tag{39}$$

where independent values of S and U are generated for each term of the sum. The amplitude $z/n\sigma_N^2$ is then compared with the threshold $T/n\sigma_N^2$ to declare a hit or a miss. Note that both $z/n\sigma_N^2$ and $T/n\sigma_N^2$ are independent of the values of n and σ_N so that the probability of detection is only a function of the probability of false alarm, the mean signal-to-noise ratio per dwell, and the number of dwells per scan.

The accuracy of the Monte Carlo technique can be checked by generating the probability of detection for the case of a single dwell per scan and comparing the result with that calculated from Equation 34. In this case the results for both small and large coherence bandwidth should be identical.

General Channel Coherence Bandwidth. Intermediate between the large and the small channel coherence bandwidth cases are propagation environments where the dwell-to-dwell transmission frequency changes partially decorrelate the propagation effects. Slow fading is again assumed so that the propagation effects are constant for the duration of a dwell. Once the m correlated samples S_i have been obtained, Equation 39 is used to calculate the noncoherently integrated amplitude $z/n\sigma_N^2$. It is convenient in this situation to generate the correlated samples of S for the three SBR geometries from the underlying normally distributed one-way voltage.

It is known (Fante, 1975) that after propagation one-way through a strongly turbulent layer, the received voltage of an initially constant amplitude and phase signal can be expressed as the sum of quadrature components

$$E_k = I_k + iQ_k \tag{40}$$

where E_k is the complex received voltage on the kth dwell with in-phase component I_k and quadrature-phase component Q_k. The components of E_k are independent, normally distributed variates with zero mean and variance equal to 1/2 so that, in the one-way propagation case, the power

$$S_{k,1} = I_k^2 + Q_k^2 \quad , \tag{41}$$

has an exponential probability density function with mean of unity.

A simple method to obtain m correlated samples of E_k is to generate a Markov process (Mitchell, 1976)

$$\begin{aligned} E_1 &= \zeta_1 \\ E_k &= \rho\, E_{k-1} + \sqrt{1-\rho^2}\, \zeta_k \quad , \quad 1 < k \leq m \end{aligned} \tag{42}$$

where $\{\zeta_k\}$ is a sequence of complex, independent samples with first-order statistics identical to those of $\{E_k\}$. It is then straightforward to show that the autocorrelation function of the sequence $\{E_k\}$ is

$$\langle E_k E_\ell^* \rangle = \rho^{|k-\ell|} \quad . \tag{43}$$

Once the correlated sequence $\{E_k\}$ has been generated with statistics appropriate to the one-way propagation case, the sequence of resulting values of power is then available for the monostatic SBR geometry. An additional sequence is necessary for the bistatic SBR configuration. The values of S_k, $1 \leq k \leq m$, for the m dwells of a scan are then given by

$$S_k = \begin{cases} S_{k,1} & \text{one-way} \\ \frac{1}{2} S_{k,1}^2 & \text{monostatic} \\ S_{k,1} S_{k,2} & \text{bistatic} \end{cases} \qquad (44)$$

where $S_{k,2}$ is an independent power appropriate to the second one-way path of the bistatic geometry.

Results. Figures 8-10 show the probability of detection during slow fading for the three cases of ω_{coh} under consideration. The results are shown as a function of signal-to-noise ratio and the number of dwells per scan, m. A check of the results is made possible by comparison of the detection curve for one dwell per scan to the appropriate detection curves for slow fading shown in Figure 4. As can be seen, the results are identical in all cases. Figures 8a-c show the probability of detection for one-way, monostatic, and bistatic propagation geometries, respectively. Because the probability of detection is insensitive to the number of dwells per scan, only results for $m = 1$, 4, and 16 are shown. These results and those for 2 or 8 dwells per scan are summarized in Table 1, which gives the probability of detection as a function of the mean signal-to-noise ratio per scan. It can be seen from the table that for probabilities of detection in the range 0.5 to 0.95 where the SBR would normally be expected to operate, the optimum detection performance is achieved with four dwells per scan. However, the difference is slight between the cases of 2 and 4 dwells per scan. An inspection of the figures shows that, for a given probability of detection above about 0.7, the one dwell per scan waveform requires the highest signal-to-noise ratio. At a probability of detection of 0.9, the difference in the required signal-to-noise ratio between the case of one dwell and of four dwells per scan is 2.5 dB for the one-way and bistatic geometries and is 2 dB for the monostatic geometry.

Table 1. Probability of detection* under slow Rayleigh fading conditions with a large frequency coherence bandwidth.

a). One-Way Geometry

Mean SNR dB/Scan	Dwells/Scan				
	1	2	4	8	16
0.00	5.755E-03	2.038E-03	5.499E-04	1.189E-04	2.453E-05
5.00	5.828E-02	3.848E-02	2.102E-02	9.139E-03	3.031E-03
10.00	2.314E-01	2.172E-01	1.838E-01	1.378E-01	8.900E-02
15.00	4.916E-01	5.245E-01	5.204E-01	4.835E-01	4.203E-01
20.00	7.241E-01	7.802E-01	7.955E-01	7.829E-01	7.501E-01
25.00	8.698E-01	9.154E-01	9.270E-01	9.237E-01	9.117E-01
30.00	9.438E-01	9.704E-01	9.755E-01	9.749E-01	9.710E-01
35.00	9.773E-01	9.897E-01	9.916E-01	9.918E-01	9.907E-01
40.00	9.912E-01	9.961E-01	9.968E-01	9.972E-01	9.970E-01

b). Monostatic Geometry

Mean SNR dB/Scan	Dwells/Scan				
	1	2	4	8	16
0.00	1.389E-02	9.401E-03	5.730E-03	3.103E-03	1.464E-03
5.00	6.137E-02	5.299E-02	4.218E-02	3.075E-02	2.032E-02
10.00	1.679E-01	1.651E-01	1.511E-01	1.293E-01	1.035E-01
15.00	3.264E-01	3.395E-01	3.311E-01	3.068E-01	2.720E-01
20.00	5.017E-01	5.294E-01	5.287E-01	5.091E-01	4.768E-01
25.00	6.585E-01	6.914E-01	6.948E-01	6.816E-01	6.575E-01
30.00	7.796E-01	8.090E-01	8.131E-01	8.051E-01	7.892E-01
35.00	8.638E-01	8.860E-01	8.894E-01	8.848E-01	8.751E-01
40.00	9.184E-01	9.334E-01	9.357E-01	9.333E-01	9.276E-01

c) Bistatic Geometry

Mean SNR dB/Scan	Dwells/Scan				
	1	2	4	8	16
0.00	1.114E-02	6.538E-03	3.363E-03	1.495E-03	5.620E-04
5.00	6.137E-02	4.957E-02	3.640E-02	2.405E-02	1.408E-02
10.00	1.897E-01	1.831E-01	1.635E-01	1.350E-01	1.027E-01
15.00	3.876E-01	4.045E-01	3.945E-01	3.634E-01	3.180E-01
20.00	5.971E-01	6.354E-01	6.385E-01	6.176E-01	5.798E-01
25.00	7.657E-01	8.078E-01	8.158E-01	8.053E-01	7.826E-01
30.00	8.768E-01	9.096E-01	9.162E-01	9.119E-01	9.007E-01
35.00	9.402E-01	9.607E-01	9.646E-01	9.631E-01	9.583E-01
40.00	9.727E-01	9.836E-01	9.855E-01	9.853E-01	9.835E-01

*Swerling 2 Target $P_{fa} = 10^{-6}$

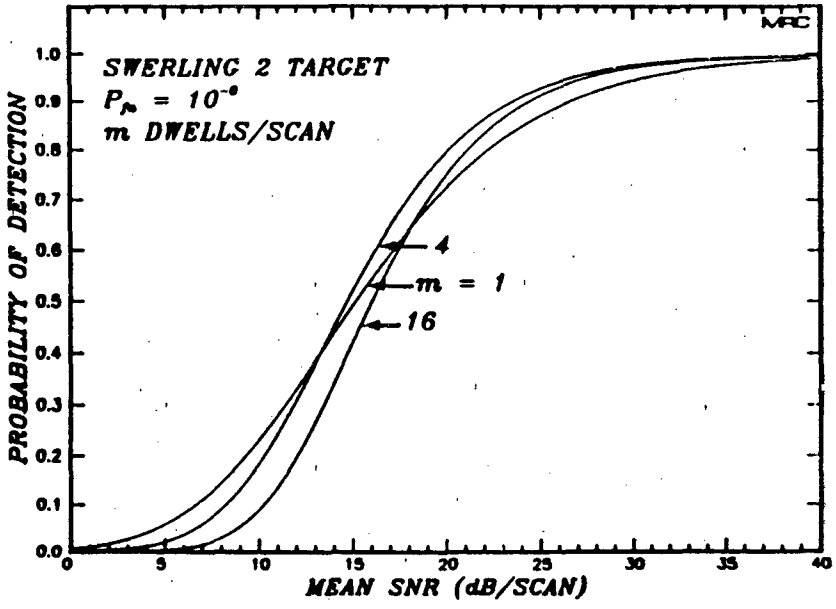

Figure 8(a). Probability of detecting a Swerling 2 target for a one-way SBR geometry, $\omega_{coh} > \omega_{hop}$.

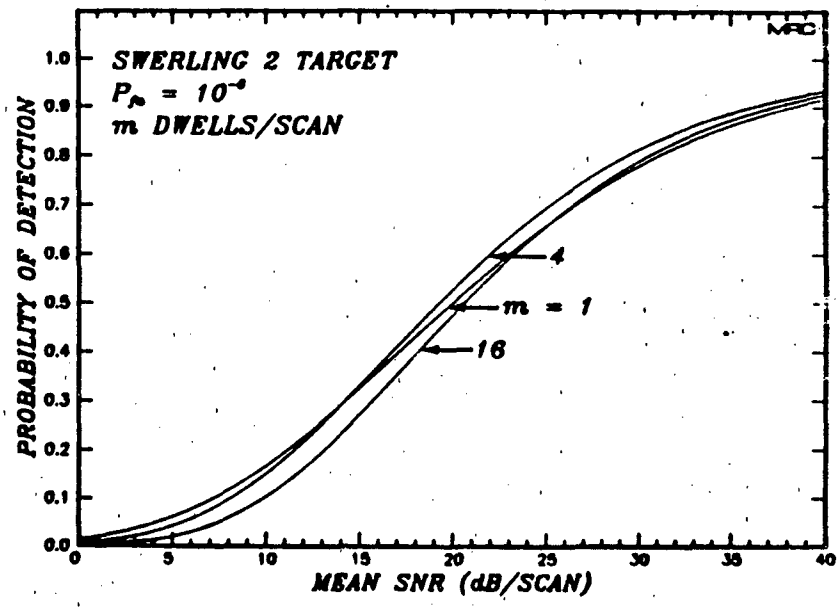

Figure 8(b). Probability of detecting a Swerling 2 target for a monostatic SBR geometry, $\omega_{coh} > \omega_{hop}$.

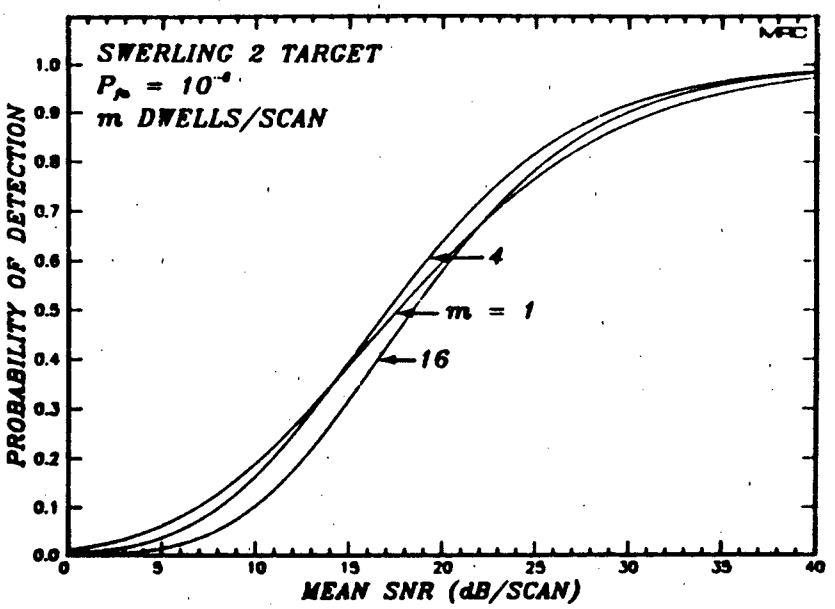

Figure 8(c). Probability of detecting a Swerling 2 target for a bistatic SBR geometry, $\omega_{coh} > \omega_{hop}$.

The detection curves for small coherence bandwidth are shown in Figures 9a-c for one-way, monostatic, and bistatic propagation geometries, respectively. The simulation results are shown as dots connected by straight lines. For one dwell per scan, close agreement is seen between analytical results (solid line) and the simulation results (stars). These detection curves have the same qualitative appearance as those for a Swerling 2 target in the absence of propagation fading. That is, at signal-to-noise ratios per scan above 15 dB or so, increasing the number of dwells per scan increases the probability of detection at the expense of giving a less graceful degradation of the probability of detection as the signal-to-noise ratio is reduced. If the criterion for defining the optimum number of dwells per scan that was used earlier for a Swerling 2 target in an ambient environment is again applied, the optimum number of

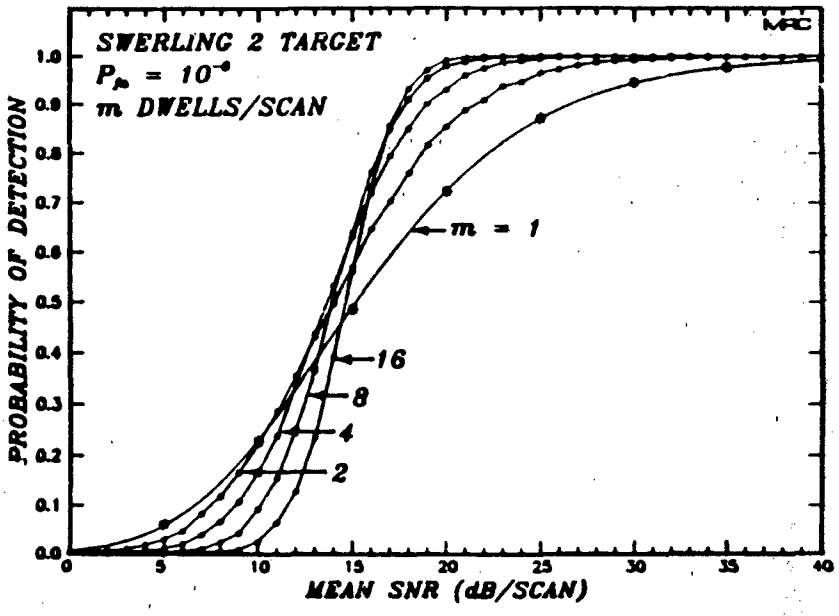

Figure 9(a). Probability of detecting a Swerling 2 target for a one-way SBR geometry, $\omega_{coh} \ll \omega_{hop}$.

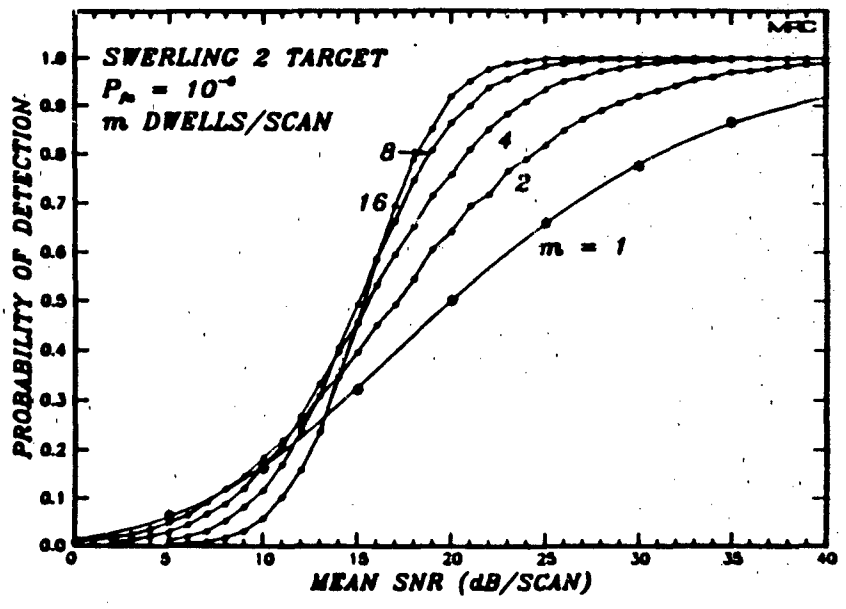

Figure 9(b). Probability of detecting a Swerling 2 target for a monostatic SBR geometry, $\omega_{coh} \ll \omega_{hop}$.

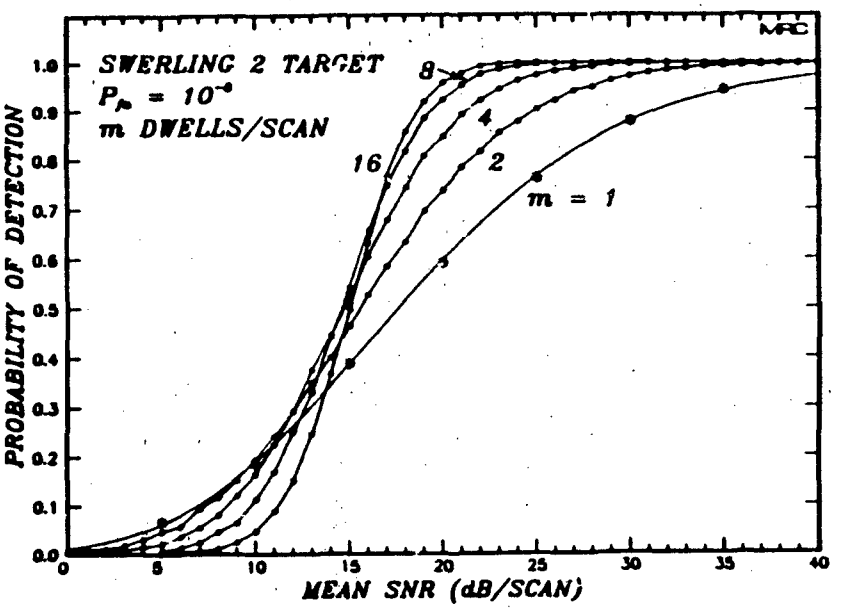

Figure 9(c). Probability of detecting a Swerling 2 target for a bistatic SBR geometry, $\omega_{coh} \ll \omega_{hop}$.

dwells per scan for $\omega_{coh} \ll \omega_{hop}$ lies between 4 and 8. Of course, as discussed previously, other design considerations might force the use of fewer than the optimum number of dwells determined on the basis of detectability alone.

Figures 10a-c show the effects of partial decorrelation of the propagation channel between dwells for the three SBR geometries. The probability of detection versus the mean signal-to-noise ratio per scan is shown for 8 dwells per scan with the correlation coefficient defined in Equation 42, ranging from 1 (which corresponds to $\omega_{coh} \gg \omega_{hop}$) to 0 (which corresponds to $\omega_{coh} \ll \omega_{hop}$). The probability of detection with 8 dwells per scan in an ambient environment is also shown. These results show that only a small amount of inter-dwell decorrelation of the fading effects is necessary to substantially improve target detectability in comparison to the case of no decorrelation. For example, at a probability

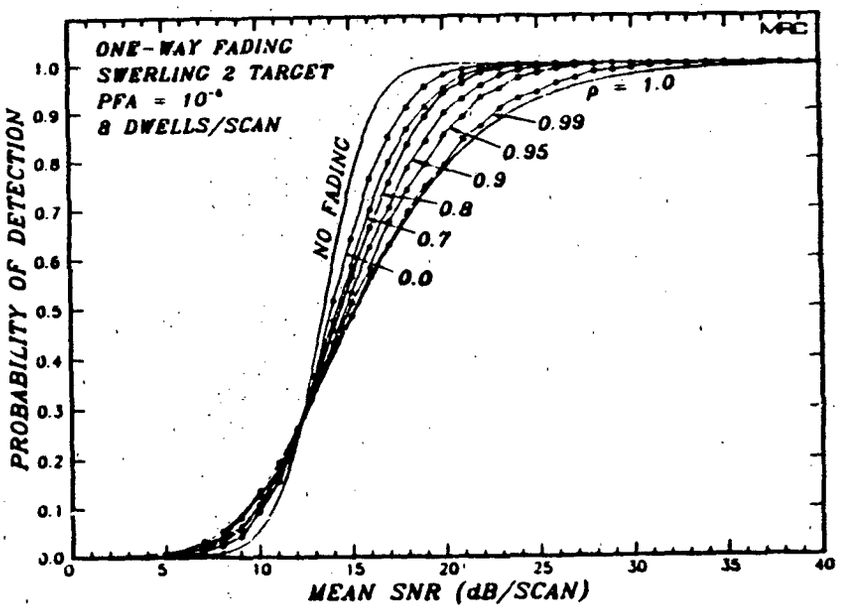

Figure 10(a). Probability of detecting a Swerling 2 target for a one-way SBR geometry characterized by dwell-to-dwell correlation.

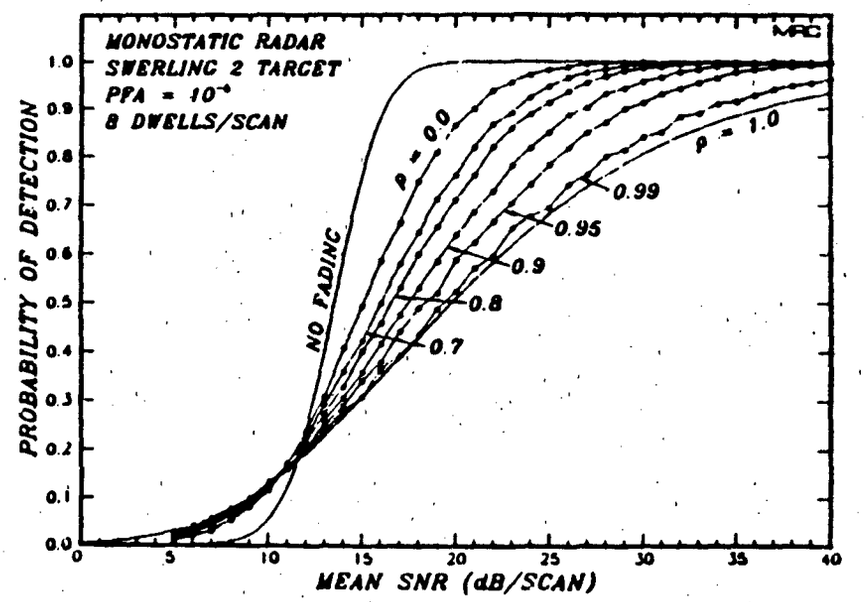

Figure 10(b). Probability of detecting a Swerling 2 target for a monostatic SBR geometry characterized by dwell-to-dwell correlation.

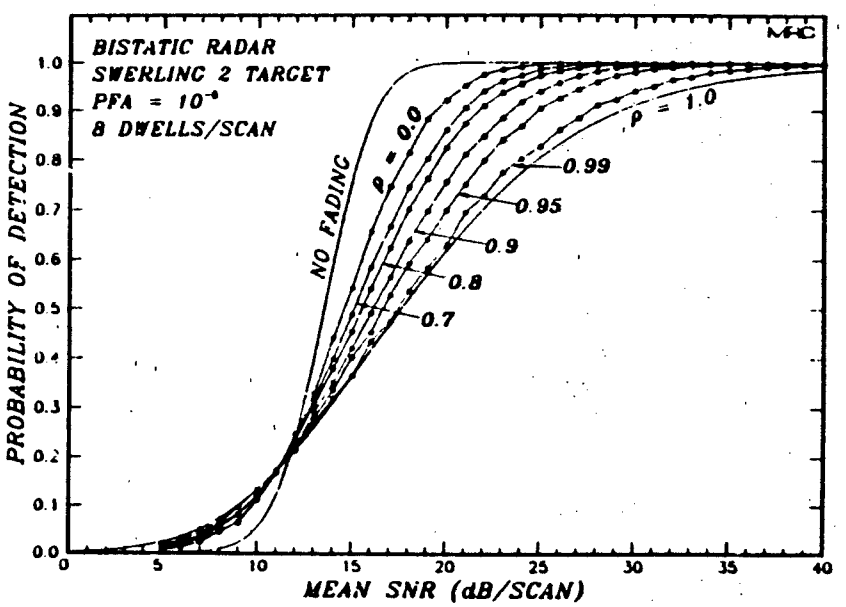

Figure 10(c). Probability of detecting a Swerling 2 target for a bistatic SBR geometry characterized by dwell-to-dwell correlation.

of detection of 0.7, a monostatic SBR that utilizes 8 dwells per scan will suffer losses in detection sensitivity of 2.7 dB for $\rho = 0$, 4.9 dB for $\rho = 0.8$, and 11 dB for $\rho = 1$. While it is apparent that the use of multiple dwells per scan does not improve detection performance in a slow fading, large coherence bandwidth channel, only a small amount of dwell-to-dwell decorrelation of the scintillation effects substantially improves detection performance.

SECTION 5
CONCLUSIONS

It is apparent that severe fading has a dramatic effect on the target detection performance of an SBR. For slow fading, when there is no degradation to the SBR coherent integration process, the losses in detection sensitivity are 7 dB for bistatic operation and 11 dB for monostatic operation. For fast fading, severe degradation occurs when the signal decorrelation time becomes smaller than about a tenth of the SBR coherent integration time. A design alternative useful for fast fading might involve adaptively changing the dwell duration so that the SBR coherent integration time does not exceed the signal decorrelation time.

When the total signal-to-noise ratio per scan for the detection of targets is fixed, the optimum detection performance in ambient or slow fading conditions is achieved when the radar energy is divided into 2 to 8 dwells per scan. Each dwell must use a separate transmission frequency so that Swerling 2 radar cross section statistics apply. Utilization of more dwells per scan enhances the detection performance at high signal-to-noise ratios at the expense of detection curves that degrade less gracefully as the signal power decreases.

When multiple dwells per scan are used during slow fading, the detection performance is sensitive to the coherence bandwidth of the propagation channel. For example, for an 8 dwell per scan waveform and at a probability of detection of 0.7, the difference in detection sensitivity

between the worst case large coherence bandwidth environment where propagation effects are constant during the scan, and the best case small coherence bandwidth environment where scintillation effects give independent voltages from dwell-to-dwell, is 8 dB for a monostatic radar and 5.5 dB for a bistatic radar. However, only a small amount of dwell-to-dwell correlation of the scintillation is necessary to achieve most of this detection sensitivity gain. It is then apparent that an SBR should attempt to maintain a large enough transmission frequency separation between dwells to insure that the scintillation effects partially decorrelate from dwell-to-dwell. Hence, an SBR measurement of the channel bandwidth appears a useful mitigation tool.

Both mitigation techniques suggested here will affect other aspects of SBR performance and require further investigation in the context of a complete SBR system.

REFERENCES

Abramowitz, M., and I. A. Stegun, Handbook of Mathematical Functions, Dover, New York, 1965.

Arendt, P. R., and H. Soicher, "Effects of Arctic Nuclear Explosions on Satellite Radio Communication," Proc. IEEE, Vol. 52, No. 6, pp. 672-676, June 1964.

Bogusch, R. L., F. W. Guigliano, D. L. Knepp and A. H. Michelet, "Frequency Selective Propagation Effects on Spread Spectrum Communications," Proc. IEEE, Vol. 69, No. 7, pp. 787-796, July 1981.

Campbell, G. A., and R. M. Foster, Fourier Integrals for Practical Applications, D. Van Nostrand Company, Inc., Princeton, New Jersey, 1948.

Dana, R. A., and D. L. Knepp, "The Impact of Strong Scintillation on Space Based Radar Design, I. Coherent Detection," IEEE Trans. Aeros. Elect. Sys., Vol. AES-19, No. 4, pp. 539-549, July 1983.

Davis, T. N., G. J. Romick, E. M. Westcott, R. A. Jeffries, D. M. Kerr, and H. M. Peek, "Observations of the Development of Striations in Large Barium Clouds," Planet. Space Sci., Vol. 22, p. 67, 1974.

Fante, R. L., "Some New Results on Propagation of Electromagnetic Waves in Strongly Turbulent Media," IEEE Trans. Antennas Propagat., Vol. AP-23, pp. 382-385, May 1975.

Fremouw, E. J., R. L. Leadabrand, R. C. Livingston, M. D. Cousins, C. L. Rino, B. C. Fair and R. A. Long, "Early Results from the DNA Wideband Satellite Experiment-Complex Signal Scintillation," Radio Science, Vol. 13, No. 1, pp. 167-187, January-February 1978.

Gradshteyn, I. S., and I. M. Ryzhik, Table of Integrals, Series, and Products, Academic Press, New York, 1965.

King, M. A., and P. B. Fleming, "An Overview of the Effects of Nuclear Weapons on Communications Capabilities," Signal, pp. 59-66, January 1980.

Knepp, D. L., Multiple Phase-Screen Propagation Analysis for Defense Satellite Communications System, DNA 4424T, MRC-R-332, Mission Research Corporation, September 1977.

Knepp, D. L., "Analytic Solution for the Two-Frequency Mutual Coherence Function for Spherical Wave Propagation," Radio Science, Vol. 18, No. 4, pp. 535-549, July-August 1983.

Knepp, D. L., Propagation of Wide Bandwidth Signals Through Strongly Turbulent Ionized Media, DNA-TR-81-78, MRC-R-671, Mission Research Corporation, March 1982.

Marshall, J, "PLACES-A Structured Ionospheric Plasma Experiment for Satellite System Effects Simulation," AIAA 20th Aerospace Sciences Meeting, Orlando, Florida, January, 1982.

Mitchell, R. L., Radar Signal Simulation, Artech House, Dedham, Massachusetts, 1976.

Papoulis, A., Probability, Random Variables, and Stochastic Processes, McGraw Hill, New York, 1965.

Pope, J. H., and R. B. Fritz, "High Latitude Scintillation Effects on Very High Frequency (VHF) and S-band Satellite Transmissions," Indian J. of Pure and Applied Physics, Vol. 9, pp. 593-600, August 1971.

Skinner, N. J., R. F. Kelleher, J. B. Hacking and C. W. Benson, "Scintillation Fading of Signals in the SHF Band," Nature (Phys. Sci.), Vol. 232, pp. 19-21, July 5, 1971.

Swerling, P., "Probability of Detection for Fluctuating Targets," IRE Trans. Info. Theory, Vol. IT-6, No. 271, pp. 273-308, April 1960.

Taur, R. R., "Simultaneous 1.5- and 4-GHz Ionospheric Scintillation Measurements," Radio Science, Vol. 11, pp. 1029-1036, December 1976.

Wittwer, L. A., A Trans-Ionospheric Signal Specification for Satellite C^3 Applications, DNA 5662D, Defense Nuclear Agency, December 1980.

Wolcott, J. H., D. J. Simons, T. E. Eastman, and T. J. Fitzgerald, "Characteristics of Late-Time Striations Observed During Operation STRESS," Effect of the Ionosphere on Space and Terrestrial Systems, J. M. Goodman, Ed., U.S. Government Printing Office, pp. 602-613, 1978.

DISTRIBUTION LIST

DEPARTMENT OF DEFENSE

Assistant to the Secretary of Defense, Atomic Energy
ATTN: Executive Assistant

Defense Advanced Rsch Proj Agency
ATTN: GSD, R Alewene
ATTN: STO, W. Kurowski

Defense Communications Agency
ATTN: Code 230
ATTN: Code 205

Defense Communications Engineer Center
ATTN: Code R410
ATTN: Code R123, Tech Library

Defense Nuclear Agency
ATTN: RAAE, P. Lunn
3 cy ATTN: RAAE
4 cy ATTN: STTI/CA

Defense Technical Information Center
12 cy ATTN: DD

Field Command
DNA, Det 1
Lawrence Livermore National Lab
ATTN: FC-1

Field Command
Defense Nuclear Agency
ATTN: FCPR
ATTN: FCTT, W. Summa
ATT FCTXE

Interservice Nuclear Weapons School
ATTN: TTV

Joint Chiefs of Staff
ATTN: C3S Evaluation Office, HDOO

Joint Data System Support Ctr
ATTN: C-312, R. Mason

Joint Strat Tgt Planning Staff
ATTN: JLAA
ATTN: JLKS
ATTN: JPTM

Under Secy of Def for Rsch & Engrg
ATTN: Strat & Theater Nuc Forces, B. Stephan
ATTN: Defensive Systems
ATTN: Strategic & Space Sys (OS)

DEPARTMENT OF THE ARMY

Atmospheric Sciences Laboratory
ATTN: DELAS-AS, H. Holt
ATTN: DELAS-EO, F. Niles

BMD Advanced Technology Center
ATTN: ATC-T, M. Capps

US Army Foreign Science & Tech Ctr
ATTN: DRXST-SD

DEPARTMENT OF THE ARMY (Continued)

BMD Systems Command
ATTN: BMDSC-LEE, R. Bradshaw
ATTN: BMDATC-R, W. Dickerson
2 cy ATTN: BMDSC-HW

Harry Diamond Laboratories
ATTN: DELHD-NW-P
ATTN: DELHD-TA-L, Tech Library

US Army Materiel Dev & Readiness Cmd
ATTN: DRCLDC, J. Bender

US Army Nuclear & Chemical Agency
ATTN: Library

US Army TRADOC Sys Analysis Actvy
ATTN: ATAA-PL

USA Missile Command
ATTN: DRSMI-YSO, J. Gamble
2 cy ATTN: Redstone Scientific Info Ctr

DEPARTMENT OF THE NAVY

Naval Electronic Systems Command
ATTN: PME-106, F. Diederich
ATTN: Code 501A

Naval Research Laboratory
ATTN: Code 4108, E. Szuszewicz
ATTN: Code 5300
ATTN: Code 4701
ATTN: Code 2627, Tech Library
ATTN: Code 4700
ATTN: Code 2000, J. Brown
ATTN: Code 6730, E. McClean
ATTN: Code 6700, T. Coffey

Naval Surface Weapons Center
ATTN: Code F31

Strategic Systems Project Office
ATTN: NSP-43, Tech Library
ATTN: NSP-2141
ATTN: NSP-2722

DEPARTMENT OF THE AIR FORCE

Air Force Geophysics Laboratory
ATTN: LYD, K. Champion
ATTN: OPR-1
ATTN: CA, A. Stair
ATTN: R. Babcock

Air Force Space Technology Ctr
ATTN: YH

Air Force Weapons Laboratory
ATTN: SUL
ATTN: CA
ATTN: NTCA

Air University Library
ATTN: AUL-LSE

DEPARTMENT OF THE AIR FORCE (Continued)

Ballistic Missile Office/DAA
ATTN: ENEF
ATTN: HQ Space Div/RSP
ATTN: ENBE

Deputy Chief of Staff
Research, Development & Acq
ATTN: AFRDS, Space Sys & C3 Dir

Rome Air Development Center
ATTN: OCS, V. Coyne
ATTN: OCSA, R. Schneible
ATTN: TSLD

Rome Air Development Center
ATTN: EEPS, P. Kossey

Space Command
ATTN: DC, T. Long

Space Division
ATTN: XPSD, J. Hatlelid

Space Division
ATTN: YGJ

Strategic Air Command
ATTN: XPFS
ATTN: XPFR
ATTN: NRI/STINFO Library
ATTN: DOTN
ATTN: DOTP
ATTN: ADWA

DEPARTMENT OF ENERGY

Department of Energy
EG&G, Inc
Attention Document Control for
ATTN: J. Colvin
ATTN: D. Wright

Department of Energy
University of California
Lawrence Livermore National Lab
ATTN: L-97, T. Donich

Department of Energy
Los Alamos National Laboratory
ATTN: MS 670, J. Malik
ATTN: T. Kunkle, ESS-5

Department of Energy
Sandia National Laboratories
ATTN: Org 1250, W. Brown
ATTN: Tech Library 3141
ATTN: D. Thornbrough
ATTN: Org 7112, C. Mehl
ATTN: C. Williams

OTHER GOVERNMENT AGENCIES

Department of Commerce
National Oceanic & Atmospheric Admin
ATTN: D. Williams

Institute for Telecommunications Sciences
National Telecommunications & Info Admin
ATTN: W. Utlaut

DEPARTMENT OF DEFENSE CONTRACTORS

Aerospace Corp
ATTN: D. Whelan
ATTN: I. Garfunkel
ATTN: J. Kluck
ATTN: G. Anderson
ATTN: V. Josephson
ATTN: A. Morse
ATTN: J. Bailey

Aerospace Corp
ATTN: S. McWaters

Analytical Systems Engineering Corp
ATTN: Radio Sciences

Electrospace Systems, Inc
ATTN: H. Logston
ATTN: P. Phillips

EOS Technologies, Inc
ATTN: B. Gabbard
ATTN: R. Lelevier

General Electric Co
ATTN: R. Juner
ATTN: R. Edsall

General Electric Co
ATTN: G. Millman

Horizons Technology, Inc
ATTN: R. Kruger

HSS, Inc
ATTN: D. Hansen

Information Science, Inc
ATTN: W. Dudziak

Institute for Defense Analyses
ATTN: E. Bauer

JAYCOR
ATTN: H. Dickinson

Kaman Sciences Corp
ATTN: J. Jordano

Kaman Sciences Corp
ATTN: E. Conrad

Kaman Tempo
ATTN: W. Schuleter
ATTN: DASIAC
ATTN: J. Devore

Kaman Tempo
ATTN: DASIAC

Lockheed Missiles & Space Co, Inc
ATTN: R. Johnson

Lockheed Missiles & Space Co, Inc
2 cy ATTN: D. Churchill

Maxim Technologies, Inc
ATTN: R. Morganstern
ATTN: E. Tsui
ATTN: J. Marshall

DEPARTMENT OF DEFENSE CONTRACTORS (Continued)

M. I. T. Lincoln Lab
ATTN: V. Vitto
ATTN: D. Towle
ATTN: J. Evans
ATTN: N. Donerty

McDonnell Douglas Corp
ATTN: R. Halprin

Mission Research Corp
ATTN: R. Christian
ATTN: R. Kilb
ATTN: M. Scheibe
ATTN: Tech Library
ATTN: C. Longmire
ATTN: F. Fajen
2 cy ATTN: D. Knepp
2 cy ATTN: R. Dana
5 cy ATTN: Document Control

Mitre Corp
ATTN: W. Foster
ATTN: W. Hall

Pacific-Sierra Research Corp
ATTN: H. Brode, Chairman SAGE

Physical Dynamics, Inc
ATTN: E. Fremouw

Raytheon Co
ATTN: G. Thome

SRI International
ATTN: F. Perkins

Swerling, Manasse & Smith, Inc
ATTN: R. Manasse

DEPARTMENT OF DEFENSE CONTRACTORS (Continued)

R&D Associates
ATTN: G. Stcyr
ATTN: R. Turco
ATTN: F. Gilmore
ATTN: H. Ory

Rand Corp
ATTN: P. Davis
ATTN: C. Crain

Rand Corp
ATTN: B. Bennett

Riverside Research Institute
ATTN: V. Trapani

Science Applications, Inc
ATTN: C. Smith
ATTN: R. Lee
ATTN: D. Hamlin
ATTN: L. Linson

SRI International
ATTN: M. Baron
ATTN: R. Leonard
ATTN: R. Leadabrand
ATTN: W. Chesnut
ATTN: J. Depp
ATTN: A. Burns

Teledyne Brown Engineering
ATTN: F. Leopard
ATTN: N. Passino

Toyon Research Corp
ATTN: J. Garbarino

END

FILMED

5-85

DTIC